JACS
JOURNAL OF THE AMERICAN CHEMICAL SOCIETY
Article
pubs.acs.org/JACS

Heterogeneous Kinetics of the Carbon Monoxide Association and Dissociation Reaction to Nitrophorin 4 and 7 Coincide with Structural Heterogeneity of the Gate-Loop

Stefania Abbruzzetti,[†] Chunmao He,[‡] Hideaki Ogata,[‡] Stefano Bruno,[§] Cristiano Viappiani,*[,†] and Markus Knipp*[,‡]

[†]Dipartimento di Fisica, Università degli Studi di Parma, and NEST Istituto di Nanoscienze CNR, viale delle Scienze 7A, I-43124, Parma, Italy

[‡]Max-Planck-Institut für Bioanorganische Chemie, Stiftstrasse 34-36, D-45470 Mülheim an der Ruhr, Germany

[§]Dipartimento di Biologia Molecolare, Università degli Studi di Parma, viale delle Scienze 23A, I-43124, Parma, Italy

Supporting Information

ABSTRACT: NO is an important signaling molecule in human tissue. However, the mechanisms by which this molecule is controlled and directed are currently little understood. Nitrophorins (NPs) comprise a group of ferriheme proteins originating from blood-sucking insects that are tailored to protect and deliver NO via coordination to and release from the heme iron. Therefore, the kinetics of the association and dissociation reactions were studied in this work using the ferroheme−CO complexes of NP4, NP4(D30N), and NP7 as isoelectronic models for the ferriheme−NO complexes. The kinetic measurements performed by nanosecond laser-flash-photolysis and stopped-flow are accompanied by resonance Raman and FT-IR spectroscopy to characterize the carbonyl species. Careful analysis of the CO rebinding kinetics reveals that in NP4 and, to a larger extent, NP7 internal gas binding cavities are located, which temporarily trap photodissociated ligands. Moreover, changes in the free energy barriers throughout the rebinding and release pathway upon increase of the pH are surprisingly small in case of NP4. Also in case of NP4, a heterogeneous kinetic trace is obtained at pH 7.5, which corresponds to the presence of two carbonyl species in the heme cavity that are seen in vibrational spectroscopy and that are due to the change of the distal heme pocket polarity. Quantification of the two species from FT-IR spectra allowed the fitting of the kinetic traces as two processes, corresponding to the previously reported open and closed conformation of the A-B and G-H loops. With the use of the A-B loop mutant NP4(D30N), it was confirmed that the kinetic heterogeneity is controlled by pH through the disruption of the H-bond between the Asp30 side chain and the Leu130 backbone carbonyl. Overall, this first study on the slow phase of the dynamics of diatomic gas molecule interaction with NPs comprises an important experimental contribution for the understanding of the dynamics involved in the binding/release processes of NO/CO in NPs.

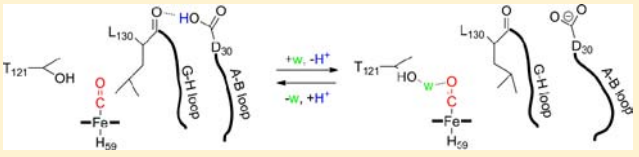

1. INTRODUCTION

Nitrophorins (NPs)[1] comprise a unique class of ferriheme proteins originating from the blood feeding insect *Rhodnius prolixus*.[2] Four NPs, designated NP1−4, were isolated from the insect saliva[3] and later recombinantly expressed.[4] Another NP, NP7, was recently established from a cDNA library and then recombinantly expressed.[5] Among the NPs, NP7 holds a special place because it is the only member among the NPs that attaches to negatively charged phospholipid membranes.[5,6] The major biological function of these proteins is the transport and delivery of NO from the insect saliva to the host tissue where NO acts as a vasodilator and blood-coagulation inhibitor.[2] The NO transport is accomplished through the binding of NO to the heme iron.[7] The protein experiences a significant pH change when subjected from the acidic pH of the saliva (5 to 6)[8] to those of the blood plasma (∼7.4) which decreases the affinity for NO.[7,9] Recently, it was established that NPs are able to produce NO from NO_2^-, which is a unique feature among ferriheme proteins.[10]

In NPs, the heme cofactor is located inside an 8-stranded β-barrel which is an unusual case for a heme protein.[11] The heme Fe is coordinated by a His, whereas the sixth coordination site is open for the binding of various ligands including the native ligands NO and histamine.[7] The protein structure has been classified as a lipocalin type of fold.[11] For NP4 and mutants derived thereof, a number of high-resolution crystal structures were obtained.[12] On the basis of these, it was proposed that an important structural feature for the functionality of NP4 is represented by the two flexible loop regions, the A-B (Glu32−Trp40) and the G-H (Lys125−Gly131) loops, which at low pH pack together to prevent NO release (closed conformation) and at high pH they depart from each other to allow NO release (open conformation). In greater detail, at low pH the loops appear in a closed conformation, although these residues have a significantly higher temperature factor compared to the

Received: December 29, 2011
Published: May 18, 2012

dx.doi.org/10.1021/ja2121662 | J. Am. Chem. Soc. 2012, 134, 9986−9998

rest of the protein. However, in the high pH structures, besides the closed conformation, electron density of an additional open conformation is obtained. The temperature factor in this case is very high for the A-B (~40−50 Å^2) and the G-H loop (~20 Å^2) and the electron density was not obtained for all atoms, which complicated the model building.[12b,c,f,13] This process is believed to be triggered in NP4 mainly by the protonation/deprotonation of Asp30 that in the protonated state H-bonds to the backbone C═O of Leu130. Consequently, the crystal structure of NP4(D30N) at pH 7.5 revealed no significant difference compared to the *wt* NP4 at pH 7.5.[12a] At low pH, *wt* NP4 closes the A-B loop of which a significant contribution is obtained from the H-bonding between Asp30:O$^{\delta}$ and the backbone C═O of Leu130. In contrast, structures of NP4(D30N) solved at pH 5.6 reveal an open conformation, indicating that protonation of Asp30 is mandatory in order to establish the respective hydrogen bond.[12a] In good agreement, kinetic parameters of NO association and dissociation did not, in contrast to *wt* NP4, significantly change between the two pH conditions.[12a] These data allow the conclusion that the pH dependent change seen for *wt* NP4, in particular for the NO affinity (K_{eq} = 2.0 × 10^7 M^{-1} (pH 5.0) → 8 × 10^6 M^{-1} (pH 8.0)), can be attributed to the pH dependent A-B loop reorientation.

In contrast to many other heme proteins, for example, myoglobin (Mb), which are reduced by excess NO,[14] NPs stabilize the Fe^{III} state through a number of carboxylate residues near the heme pocket[15] in combination with a ruffled heme geometry.[16] This way, the reduction potential is established at, for example, −303 mV versus SHE for NP1 compared to ~0 mV versus SHE for Mb.[17] The resulting stabilization of the {FeNO}^{6} complex is important for NP function because ferroheme−NO, that is, {FeNO}^{7}, association constants are too large (K_{eq}(Fe^{II}) = 10^{13}−10^{14} M^{-1})[9,15] to allow effective NO release in vivo.[18]

In a biological environment, NO is a remarkably unstable molecule with, for example, $t_{1/2}$ ≈ 100 ms in blood plasma.[19] On the other hand, although it is a signaling molecule, it is able to move across cell membranes.[20] Therefore, the question arises how the specific targeting of an NO signal is achieved in vivo. This is interesting not only for the understanding of NO biology, but also for medical reasons because NO overproduction can be dangerous,[21] where in other cases the pharmacological administration of NO to a specific target tissue is desired.[22] In this respect, the molecular mechanisms of NPs represent an interesting case to be studied as naturally occurring delivery systems for NO.

Although the principal biological function of NPs is arguably the transport and delivery of NO, the underlying molecular mechanism and the structure−function relationships remain to be elucidated. NO association reactions are very fast processes and, therefore, pose a challenge for their experimental observation. Investigation with the physiologically less important CO complexes takes advantage of the slower CO association kinetics as compared to NO association reactions to extract a more accurate determination of kinetic processes. On the other hand, Fe^{II}−CO represents a model for the isoelectronic {FeNO}^{6} so that both complexes exhibit similar ligand−heme geometries, that is, ∠(Fe−X−O) ≈ 180° (X = C,N). Furthermore, in both cases, a neutral diatomic gas molecule is released from the cofactor upon laser-flash photolysis (LFP). CO complexes of ferroheme proteins have been extensively investigated by laser-flash induced rapid scanning techniques, and thus, a wealth of data for comparison is available.[23] Therefore, this technique was applied to elucidate the kinetic properties of the NP4 and NP7 interactions with CO. These experiments were accompanied by stopped-flow kinetic measurements and by FT-IR and resonance Raman (RR) spectroscopy.

2. EXPERIMENTAL PROCEDURES

2.1. Preparation of Protein Samples. NP4, NP4(D30N), and NP7 were recombinantly expressed in *Escherichia coli* strain BL21-(DE3) (Novagen) and reconstituted as was previously described.[5b,12f] Stock solutions of $Na_2S_2O_4$ were always prepared freshly before use. The carbonyl complexes of the ferroheme proteins were prepared in closed vessels in deoxygenated solvents under a CO atmosphere. The protein was titrated with $Na_2S_2O_4$ until all protein was reduced, which was monitored by absorption spectroscopy. The preparation and handling of unliganded ferroheme proteins was carried out inside an anaerobic chamber (Coy, Inc.) with an atmosphere comprised of 98% N_2/2% H_2 in the presence of Pd catalysts. All solutions were rendered essentially O_2 free by three freeze−pump−thaw cycles performed at a vacuum line ($p < 10^{-3}$ bar).

2.2. FT-IR Spectroscopy. Samples for FT-IR spectroscopy were prepared in the anaerobic chamber upon concentrated in Ultrafree ultrafiltration concentrators (NMWL = 10 kDa; Millipore). The degassed protein solution was saturated with CO before controlled reduction with $Na_2S_2O_4$. Samples were transferred to a 50-μL gastight transmission cell equipped with CaF_2 windows. FT-IR spectra were recorded on a Bruker IFS 66v/S FTIR spectrometer equipped with an MCT photoconductive detector and a KBr beam splitter. The temperature was set to 25 °C with a thermostat (RML, LAUDA).

2.3. Resonance Raman Spectroscopy. Samples of ~100 μM of protein were reduced with $Na_2S_2O_4$ under strictly anaerobic conditions as described above in the presence of a ^{12}CO (natural isotopic abundance) or a ^{13}CO (99.19% ^{13}C) atmosphere. The samples were transferred into a sealed cylindrical cuvette (5.5 cm diameter, 3 mL volume). The integrity of the samples was monitored by the recoding of a second spectrum right after the original measurement. In the case of a significant difference, that is, indicating significant oxidation, the spectra were discarded. RR spectra were recorded with a scanning double monochromatic. The excitation line at 413.1 nm was provided by a coherent K-2 Kr^+ ion laser, and the sample was rotated throughout the measurement to minimize radiation damage. For measurements in frozen solution, samples of ~50 μM were filled into 3 mm quartz tubes and kept in a quartz Dewar filled with liquid N_2 during the measurement.

2.4. Nanosecond Laser-Flash Photolysis Experiments. The experimental setup was described in detail elsewhere.[24] Photolysis of CO complexes was obtained using the second harmonic (532 nm) of a Q-switched Nd:YAG laser (HYL-101, Quanta System). The cw output of a 75 W Xe arc lamp was used as probe beam, a 5 stages photomultiplier (Applied Photophysics) for detection and a digital oscilloscope (LeCroy LT374, 500 MHz, 4 GS s^{-1}) for digitizing the voltage signal. A spectrograph (MS257 Lot-Oriel) was used to select the monitoring wavelength (436 nm) and to remove the residual stray light from the pump laser. The sample holder is accurately temperature controlled with a Peltier element, allowing a temperature stability of better than 0.1 °C. Experiments were performed in the temperature range 10−30 °C.

Time-resolved difference absorbance spectra were measured using a gated intensified CCD (Andor Technology, iStar, 1024 × 1024 pixels used in full vertical binning mode), coupled to the spectrograph. Time-resolved spectra consist of photoproduct minus NP−CO difference spectra at 70 logarithmically spaced time delays following photodissociation, from 10 ns after the laser flash to 10 ms. Spectra are obtained by averaging 100 single shot signals at each delay.

Samples for LFP experiments were prepared by equilibrating the solutions in a sealed 1 cm-quartz cuvette connected to a tonometer with 0.1 or 1 atm CO. $Na_2S_2O_4$ was then titrated anaerobically into the solution while formation of the CO adduct was monitored by

dx.doi.org/10.1021/ja2121662 | J. Am. Chem. Soc. 2012, 134, 9986−9998

absorption spectroscopy. Inclusion of 1 mM of L-cystine in the solution significantly improved the sample stability during LFP experiments. The solubility of CO in water is such that its concentration is 1.05 mM at 10 °C when the solution is equilibrated with 1 atm CO. The temperature dependence of CO solubility[25] was taken into account in the numerical analysis. The numerical analysis of the rebinding kinetics was described in detail previously.[23b]

2.5. Stopped-Flow Kinetic Measurements. To monitor the absorption change upon rapid mixing of two reactants under anaerobic conditions, a Cary-50 absorption spectrophotometer was equipped with a fiber optic coupler (Varian, Inc.). Flexible fiber optics (Ocean Optics, Inc.) were used to connect the spectrophotometer with a cuvette holder (Ocean Optics, Inc.) inside the anaerobic chamber. Buffers were rendered essentially O_2 free by three freeze-pump cycles at a vacuum line. All of the following steps were carried out inside the anaerobic chamber. The solvent of the protein was exchanged to either 100 mM MOPS/NaOH (pH 7.5) or 100 mM NaO*Ac*/HO*Ac* (pH 5.5) and NP4 and NP7 were concentrated to 10 μM and 14 μM, respectively, using Ultrafree ultrafiltration concentrators (NMWL = 10 kDa; Millipore). A CO stock solution was prepared by saturation of water thermostatted to 20 °C with CO gas, which corresponds to a concentration of 1.0 mM.[26] Upon preparation of the ferroheme proteins, the respective CO solution was prepared by mixing of buffer with CO saturated water at various ratios. The temperature of the solutions was equilibrated in the syringes of a water-bath thermostatted UV−vis stopped flow apparatus RX.2000 equipped with a DA.1 pneumatic drive (Applied Photophysics Ltd.; dead time, 2 ms). The cuvette of the RX.2000 was inserted into the holder. Upon temperature equilibration, the protein was mixed with the substrate while the absorption was followed at 385, 404, and 421 nm. The absorbance was read every 0.1 s. The analysis of the kinetic data was performed using ORIGINPRO V7.5 (OriginLab Corporation).

In another set of experiments, the CO form of the proteins was prepared and filled into one syringe of the stopped-flow apparatus. The other syringe was filled with either 10 mM imidazole (ImH) in the respective buffer or buffer was used that was saturated with O_2 prior. In this latter case, the reaction trace was followed at 421 nm.

3. RESULTS

3.1. UV−Vis Absorption Spectroscopy of the Carbonyl Complexes of NP4 and NP7. The reduction of NP4 and NP7 is performed with $Na_2S_2O_4$. However, both proteins are sensitive to the addition of excess $Na_2S_2O_4$ because the disulfide bonds are prone to reduction as well.[27] Therefore, in order to maintain the disulfide bridges intact, the amount of reductant was limited and a scavenger disulfide (1 mM L-cystine) was applied to the solution during LFP experiments. The reduction of NP4 induces a Soret band maximum shift to 426 nm and the Q-band shifts to ~557 nm.[12b] Upon addition of CO, a sharp Soret band at 420 nm is yielded as well as Q bands at 540 and 564 nm.[12b] In case of NP7, however, two Soret bands are obtained at ~388 and ~422 nm, which is presented in Supporting Information Figure S1. It was shown that the two Soret band maxima reflect both the form with the proximal His60 bound (His-on) and the proximal His60 unbound (His-off); both forms are in slow exchange equilibrium with each other.[28] It is important to note, though, that the binding of CO induces the rebinding of His60 to Fe^{II}, which is reflected in the formation of a single sharp Soret absorption at 421 nm and the Q-bands at 538 and 569 nm. The reformation of His−Fe^{II}−CO is ascribed to the positive trans effect of CO.[29] This is also well in agreement with the previous finding that the energetic barrier between the His-on and the His-off form is small enough to allow exchange equilibrium.[28]

3.2. Vibrational Spectroscopy. Information about the coordination environment of the heme iron in the diamagnetic (S = 0) carbonyl complexes is obtained from RR spectra. For the determination of RR spectra of the Fe^{II}−CO proteins, upon careful reduction and addition of CO, samples were sealed to protect from reoxidation.[10c] Excitation was performed by laser irradiation into the Soret band absorption at 413.1 nm. The measurements were carried out at room temperature and the resulting spectra of *wt* NP4 at pH 5.5 and 7.5, of *wt* NP7 at pH 5.5 and 7.5, and of NP4(D30N) at pH 7.5 are displayed in Figure 1. The latter spectrum is relevant since the mutation

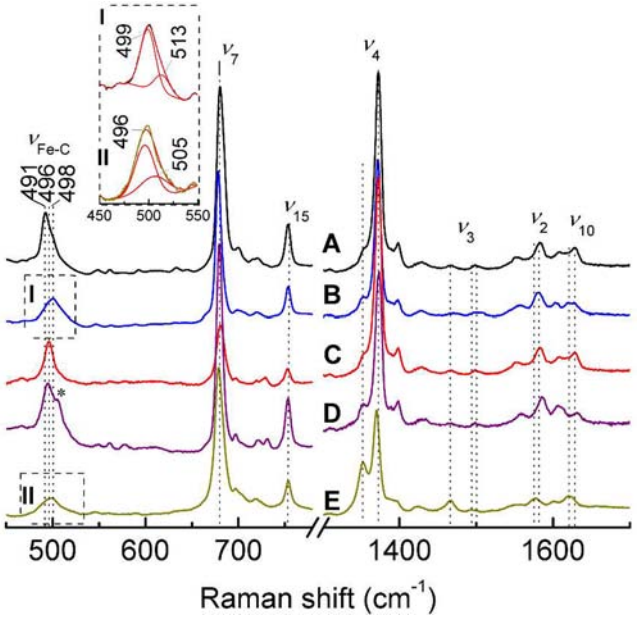

Figure 1. RR spectra of the CO complexes of (A) NP4 at pH 5.5, (B) NP4 at pH 7.5, (C) NP7 at pH 5.5, (D) NP7 at pH 7.5, and (E) NP4(D30N) at pH 7.5. (λ_{ex} = 413.1 nm; all measured at ambient temperature except for NP7, which was measured at 77 K; pH 5.5, 100 mM NaO*Ac*/HO*Ac*; pH 7.5, 100 mM MOPS/NaOH). Inset: The indicated ν_{Fe-C} band was fitted by two Gaussian functions in the case of (I) NP4 and (II) NP4(D30N). (For the assignment of ν_{Fe-C} see Supporting Information Figure S2.)

D30N is known to affect the interaction between the A-B and G-H loops.[12a,c] The most prominent core-size marker band in the high-frequency region of the RR spectra of heme proteins is the oxidation state marker ν_4 that indicates the presence of Fe^{III} (1370−1375 cm^{-1}) or Fe^{II} (1350−1375 cm^{-1}).[30] In NP4, ν_4 = 1372 cm^{-1} confirms Fe^{II}. Another important feature seen in Figure 1 is the so-called spin-state maker ν_3. The ν_3 porphyrin skeletal mode is sensitive to the heme core size, which changes with the spin state of Fe in dependence of the oxidation state, that is, 1460−1470 cm^{-1} for 5cHS Fe^{II} and 1490−1510 for 5cLS or 6cLS Fe^{II}.[30d,e,31] For NP4 and NP7, a band at 1498 and 1499 cm^{-1}, respectively, is obtained, which reflects 6c species as expected. Comparison with the spectral features of Mb shows that also the ν_2 and ν_{10} bands further support the assignment.[32] However, in both cases at the lower frequency flank of ν_4, a small resonance appears at 1353 and 1354 cm^{-1}, respectively, which originates from a small fraction of HS Fe^{III}, that is, developing from air oxidation during the spectra recording. The appearance of this band is accompanied by an additional ν_3 at 1468 cm^{-1}, which is diagnostic of 5c. In conclusion, the excitation laser yields a small fraction of the CO depleted form which can, however, be neglected.

dx.doi.org/10.1021/ja2121662 | J. Am. Chem. Soc. 2012, 134, 9986−9998

In the low-frequency part of the RR spectrum of NP4−CO, a decently intensive and sharp band at 492 cm^{-1} appears at pH 5.5 that represents the ν_{Fe-C} stretch vibration. This assignment was based on the isotopic labeling with ^{13}CO (Supporting Information Figure S2). Noticeably, this band converts into a broad band with a maximum at ∼500 cm^{-1} upon increase of the pH to 7.5, which originates from the overlapping of at least two close vibrations (see below).

Because of the symmetry related selection rules, the ν_{C-O} stretching vibration (typically at ∼1950 cm^{-1}) is low in intensity in RR spectra, but is very strong in IR spectroscopy. The lack of vibrations from the protein in this region further facilitates the detection. Therefore, FT-IR spectra of NP4−CO and NP7−CO were recorded at pH 7.5 and 5.5 at ambient temperature and are displayed in Figure 2. It was noticed before

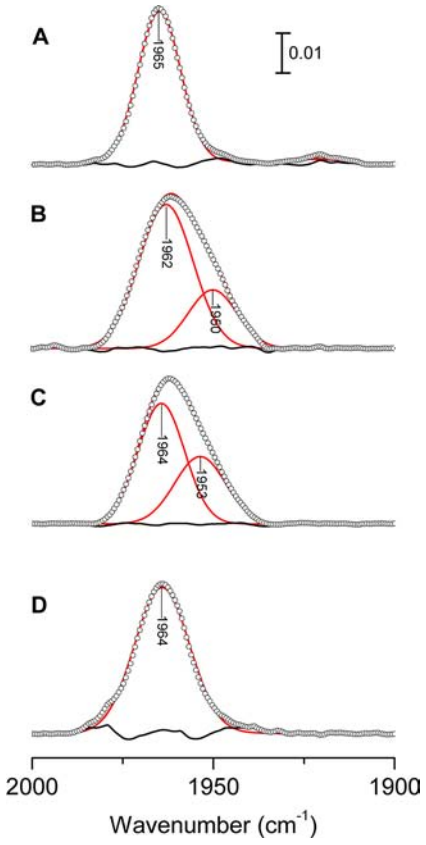

Figure 2. FT-IR spectra of the CO complexes of (A) NP4 at pH 5.5, (B) NP4 at pH 7.5, (C) NP4(D30N) at pH 7.5, and (D) NP7 at pH 7.5. Measurements were performed at ambient temperature in either 100 mM NaO*Ac*/HO*Ac* (pH 5.5) or 100 mM MOPS/NaOH (pH 7.5). Open circles represent the experimental data, which were fit by (a) Gaussian function(s) (red line). The residual is drawn in black.

that the vibrational band of NP4−CO is relatively broad, which was attributed to the coexistence of several conformers.[33] However, at pH 5.5 ν_{C-O} of NP4−CO (Figure 2A), but also of NP7−CO at pH 7.5 (Figure 2D), is fairly symmetric, whereas those of NP4−CO at pH 7.5 (Figure 2B) and NP4(D30N) (Figure 2C) exhibit a clear shoulder at the low-frequency flank. It appears that the IR band of NP4−CO at pH 5.5 and that of NP7−CO at pH 7.5 are well approximated by a single Gaussian function with maxima at 1965 and 1964 cm^{-1}, respectively. In contrast, the IR bands of the high pH species of NP4−CO are only sufficiently described by a minimum of two Gaussian functions with relative amplitudes of ∼1:4. The resulting values and selected examples from literature are reported in Supporting Information Table S1 together with the ν_{Fe-C} frequencies derived from the RR spectra (see above). The major species in NP4−CO at pH 7.5 exhibits a shift of 3 cm^{-1} compared to the sample at pH 7.5. The respective low frequency bands appear at 1950 cm^{-1} and 1955 cm^{-1}. We label these species as open (**o**) and closed (**c**) conformations (Supporting Information Table S1).

Fe^{II}−CO complexes are characterized by strong $d_\pi(Fe) \rightarrow \pi^*(CO)$ backdonation. However, the resulting increase in electron density at the antibonding $\pi^*(CO)$ orbital leads to a weakening of the C−O bond, which is reflected in the anticorrelation between ν_{Fe-C} and ν_{C-O}.[30b,34] Moreover, the frequencies depend in part on the polarity of the solvent, which in case of proteins is represented by the heme pocket. In Figure 3, the ν_{Fe-C}/ν_{C-O} pairs determined in this study are plotted

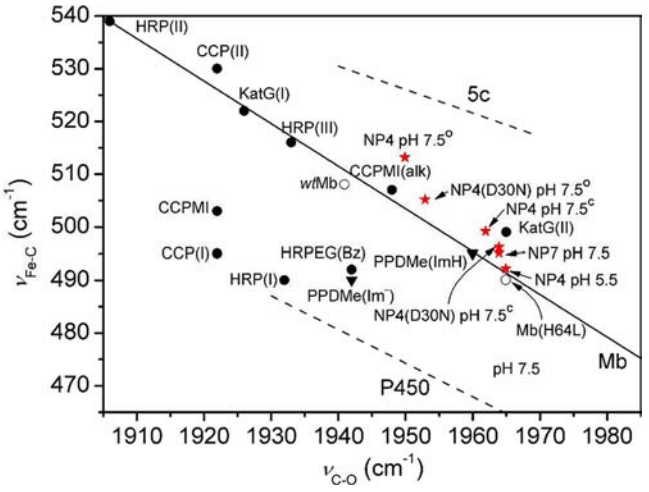

Figure 3. Anticorrelation plot of the ν_{Fe-C} versus ν_{C-O} frequencies in Fe^{II}−CO heme proteins and model complexes ligated by imidazole type of ligands. The solid line is derived from the fitting of Mb variants reported in reference 34b, two examples of which are represented by ○. Other protein examples listed in Supporting Information Table S1 are represented by ● and the model hemes by ▼. The ν_{Fe-C}/ν_{C-O} pairs determined in this study are represented by red stars. The top dashed line (5c) is derived from the fitting of frequencies determined for 5-coordinate CO adducts of derivatives of [Fe^{II}tetraphenylporphyrinate] substituted at the macrocycle.[35] The bottom dashed line is derived from the fitting of frequencies determined from CO adducts of $P450_{cam}$ with several substrates.[34b,36]

together with typical examples of His-liganded heme proteins (Supporting Information Table S1). In general, the plot indicates that all of the NPs correlate reasonably with the typical examples from literature where $His_{proximal}$ has the character of a neutral ligand. This demonstrates that the assignments for the combination of ν_{Fe-C} and ν_{C-O} vibration presented in Supporting Information Table S1 are correct. However, where the main frequency pairs $\nu_{Fe-C}{}^{c}/\nu_{C-O}{}^{c}$ assemble in a very narrow range, the frequency pairs $\nu_{Fe-C}{}^{o}/\nu_{C-O}{}^{o}$ appear at relatively different positions which are located significantly in the outlier region. In greater detail, the $\nu_{Fe-C}{}^{c}/\nu_{C-O}{}^{c}$ pairs appear at positions similar to that of Mb(H64L) which provides, in contrast to *wt* Mb, but similar to the NPs, a very hydrophobic distal heme pocket. The low-abundance forms **o** have a decreased Fe−C bond length and an increased

dx.doi.org/10.1021/ja2121662 | *J. Am. Chem. Soc.* 2012, 134, 9986−9998

C−O bond length, although the scattering of the $\nu_{Fe-C}°/\nu_{C-O}°$ pairs with respect to the normal line is relatively high. The experiments presented in the following and their discussion will help to understand the nature of form **o** (see below).

3.3. CO Rebinding upon Laser Photolysis. CO rebinding after nanosecond LFP of NP4−CO and NP7−CO at pH 5.5 and 7.5 is shown in Figure 4A. A fast and similar

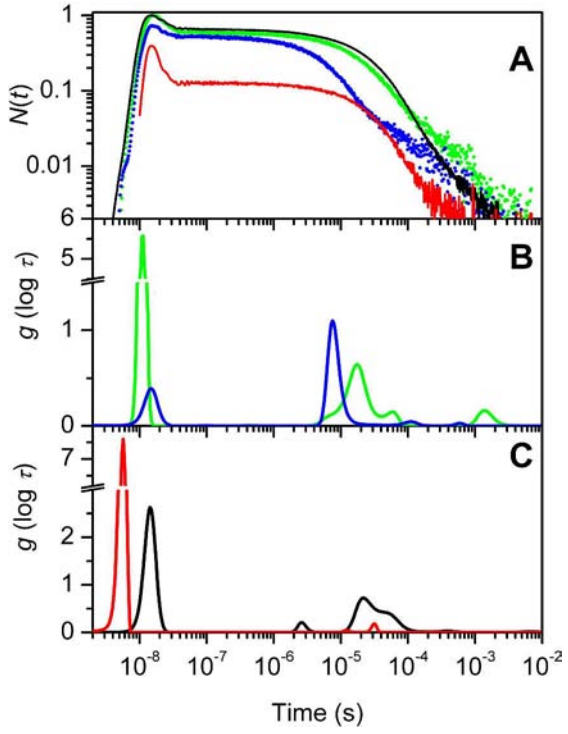

Figure 4. (A) Representative CO rebinding kinetics to NP7 (pH 7.5, green; pH 5.5, blue) and NP4 (pH 7.5, black; pH 5.5, red) in solutions equilibrated with 1 atm CO partial pressure at 25 °C. (B and C) Lifetime distributions determined from the MEM analysis of the rebinding kinetics in panel A (pH 5.5, 100 mM NaO*Ac*/HO*Ac*; pH 7.5, 100 mM MOPS/NaOH).

nanosecond geminate recombination occurs for both *wt* proteins, whose amplitude increases from about 35% at pH 7.5 to nearly 70% when the pH is lowered to 5.5. In the case of NP7, the geminate recombination becomes so fast upon lowering the pH to 5.5 that an even larger fraction of the resulting rebinding falls within the instrumental dead time (a few nanoseconds) and most of the kinetics is lost to our detection system. A heterogeneous bimolecular phase is observed for both proteins and the broadening is more pronounced at neutral pH, especially for NP7. These features are reflected in the associated lifetime distributions (Figure 4B,C), where a prominent geminate rebinding is observed at 10 ns, whose amplitude becomes higher upon lowering the pH to 5.5. Small bands peaked at ∼100 ns and ∼10 μs in the NP7 lifetime distributions are evidence of CO rebinding from temporary sites located inside the protein matrix. On the microsecond time scale, several bands are present, some of which are dependent on CO concentration (Supporting Information Figure S3), a fact that demonstrates that they are associated with bimolecular kinetics. A long-lived reaction intermediate is observed at ∼0.1 ms (NP4) and 1 ms (NP7), and the amplitude of this phase is higher at pH 7.5 and at 0.1 atm of CO.

The latter finding suggests that the slow rebinding species are formed upon relaxation of the NP4 and NP7 structures to less reactive states. At reduced CO concentration, the bimolecular CO rebinding reaction slows down, and this allows a more extensive relaxation of the unliganded structure, thus, resulting in a higher population of the slow rebinding molecular species.

Further evidence that a structural relaxation is occurring comes from the Singular Value Decomposition (SVD) analysis of time-resolved spectra, measured following photodissociation of NP7−CO, that are reported in Figure 5 (the time-resolved

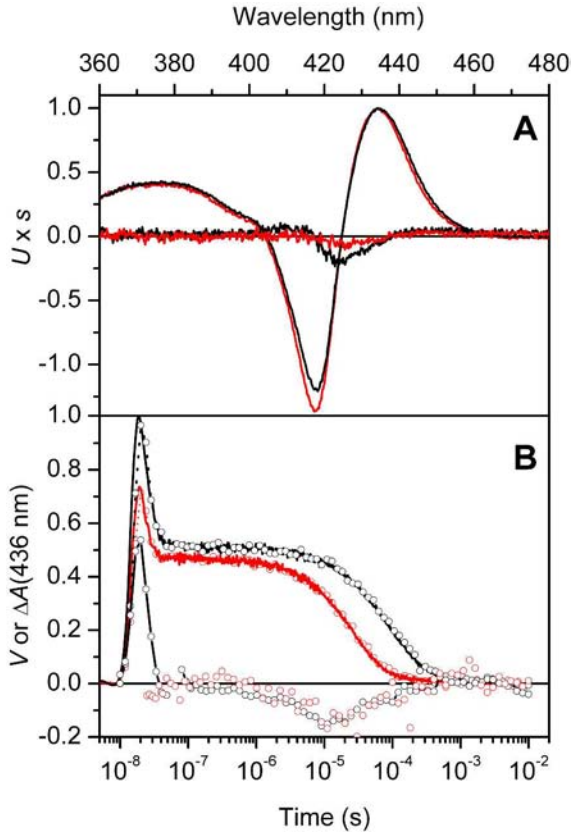

Figure 5. Meaningful spectral components (A) and amplitudes (B) retrieved from the SVD analysis of the time-resolved spectra measured after photodissociation of NP7−CO at pH 7.5 (black) and pH 5.5 (red) at 0.1 atm CO. Singular values were 7.9 and 0.3 for the spectral components at pH 7.5, and 6.3 and 0.13 at pH 5.5 (pH 5.5, 100 mM NaO*Ac*/HO*Ac*; pH 7.5, 100 mM MOPS/NaOH). The spectral components are multiplied by the corresponding singular values. The second spectral components are further multiplied by 5.

spectra for NP4−CO are available in Supporting Information Figure S4). The first spectral component (Figure 5A) closely matches the difference between the absorption spectra of NP7−CO and NP7 (NP4−CO and NP4) and the time course of the spectral amplitudes (Figure 5B) follows the same trend as the rebinding kinetics measured at 436 nm. For both proteins, a small yet appreciable second spectral component is detectable. Its amplitude has a time profile which suggests relaxation of NP7 (NP4) to a structure with a distinct spectrum on the microsecond time scale, followed by back relaxation to the liganded structure as CO is rebound. An additional relaxation is detectable in the short nanoseconds for NP7 at pH 7.5. In the case of NP4, the second spectral component is characterized by very small amplitude and the time evolution

dx.doi.org/10.1021/ja2121662 | J. Am. Chem. Soc. 2012, 134, 9986−9998

has a less clear trend. The second spectral component is smaller at pH 5.5.

3.4. Analysis of CO Rebinding Kinetics to NP4. As is presented in section 3.2, ν_{C-O} of NP4−CO at pH 7.5 occurs at two main frequencies (1950 and 1962 cm^{-1}, Supporting Information Table S1 and Figure 3), suggesting that the bound ligand experiences a heterogeneous bond strength. The existence of two subpopulations matches the finding of a heterogeneous bimolecular phase, which has to be taken into account in a quantitative kinetic model. When the pH is lowered to 5.5, the bimolecular phase becomes less heterogeneous which agrees well with a single ν_{C-O} at 1965 cm^{-1} (Supporting Information Table S1). Under these conditions, the rebinding kinetics can be described by a single static conformation, although kinetic relaxation is still observed. CO rebinding kinetics to NP4 at pH 7.5 was thus analyzed using a model with two noninterconverting conformations as outlined in Scheme 1.

Scheme 1. Extended Minimal Reaction Scheme for the Observed CO Rebinding Kinetics to NP4

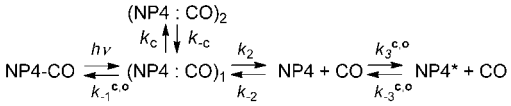

The model assumes that two conformations (**c**, for closed and **o**, for open) exist in solution, with distinct values for some of the microscopic rates (k_{-1}^{c} versusk_{-1}^{o}, k_3^{c} versus k_3^{o}, and k_{-3}^{c} versus k_{-3}^{o}) . The remaining rate constants (k_c, k_{-c}, k_2, and k_{-2}) have the same values for both conformations. The observed rebinding kinetics is described by a linear combination of the kinetics, resulting from Scheme 1, for conformation **o** and conformation **c**. The relative weights of **c** versus **o** were taken from the fitting of the FT-IR absorbance measurements. This model can describe accurately the rebinding kinetics under all tested experimental conditions, as shown in Figure 6 for representative rebinding curves at 1 atm of CO and 25 °C, at pH 5.5 and pH 7.5. The resulting microscopic rates and the corresponding activation free energies are summarized in Supporting Information Table S2.

When the rebinding kinetics is measured for the NP4-(D30N) mutant, the increase in geminate rebinding upon lowering the pH to 5.5 is not as evident as for the *wt* protein (Supporting Information Figure S7). Unlike for the *wt* protein, kinetic heterogeneity is observed at pH 7.5 and 5.5. The analysis thus requires the full reaction Scheme 1, where two populations, with different microscopic rates, are taken into account. However, the spectral change observed in the time-resolved spectra of the *wt* protein is absent for this mutant (data not shown), and the process with rates $k_{-3}^{o,c}$ and $k_3^{o,c}$ is negligible.

From the free energy barriers reported in Supporting Information Table S2, a free energy profile for the migration of the ligand is built (Figure 7) assuming a free energy of 0 for state NP4 + CO. The innermost rebinding step is characterized by slightly larger barriers for both conformations **c** and **o** at neutral pH. Barriers for exit to and return from the solvent are very similar at both pH values. The temporary docking site for CO $(NP4 : CO)_2$ is stabilized at neutral pH.

3.5. Analysis of CO Rebinding Kinetics to NP7. Unlike the case of NP4−CO, FTIR spectra of NP7−CO solutions are

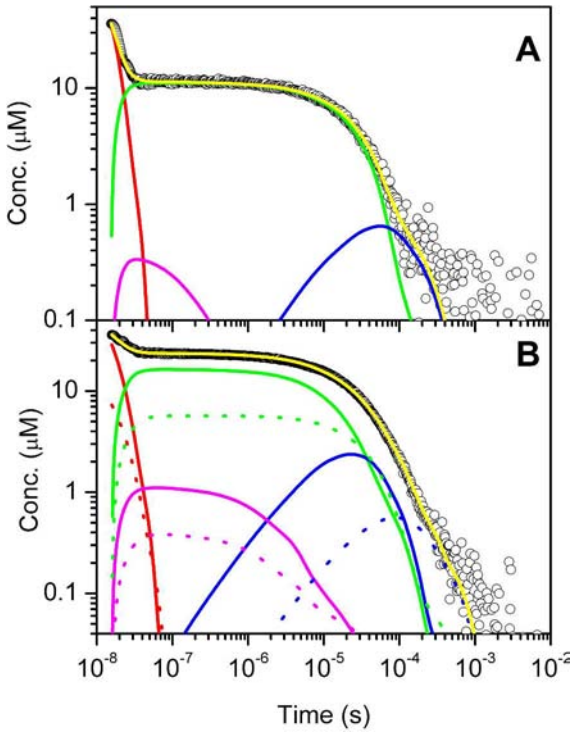

Figure 6. Representative fitting (yellow trace) with the model outlined in Scheme 1 for CO rebinding kinetics (○) to NP4 solutions at pH 5.5 (A) and pH 7.5 (B) at 25 °C and 1 atm CO. Reaction intermediates red, $(NP4 : CO)_1$; magenta, $(NP4:CO)_2$; blue, NP4*; green, NP4. Dotted and solid lines in panel B represent reaction intermediates for the 27% and the 73% components, respectively (pH 5.5, 100 mM NaO*Ac*/HO*Ac*; pH 7.5, 100 mM MOPS/NaOH).

characterized by a single ν_{C-O} both at pH 5.5 and 7.5. This is paired by the absence of substantial (static) heterogeneous rebinding kinetics. Scheme 2 is derived from Scheme 1 in which migration to an additional temporary docking site is included. In comparison to NP4, the photodissociated ligand appears to sample the internal cavities of the protein for much longer times, and the shape of the progress curve suggests that multiple (at least two) docking sites exist inside the protein matrix, from which CO is rebound at delayed times.

Analysis of the nanosecond phase for the pH 5.5 data is complicated by the extremely fast rebinding, which prevents a careful determination of the innermost rebinding (k_{-1}) and the exit (k_2) rate constants. Nevertheless, the striking increase in k_2 and in k_{-2} upon lowering the pH is a strong indication that under these conditions the ligand is exchanged much more easily between the protein matrix and the solvent.

Figure 8 reports representative fits to the CO rebinding kinetics to NP7 under selected conditions, showing also the time course of the reaction intermediates. At acidic pH, relaxation to the slow reacting species occurs to a much lower extent, and this favors rebinding, resulting in much higher apparent rates. From the curves, it also appears that the population of the second docking site shapes the progress curve and contributes substantially to the slow phase. The resulting microscopic rates and the corresponding activation free energies are summarized in Supporting Information Table S3.

The free energy profiles in Figure 7 were calculated from the free energy barriers reported in Supporting Information Table S3, assuming for NP7 + CO a free energy of 0. As for NP4, the effect of pH on the free energy barrier for rebinding (rate k_{-1})

dx.doi.org/10.1021/ja2121662 | J. Am. Chem. Soc. 2012, 134, 9986−9998

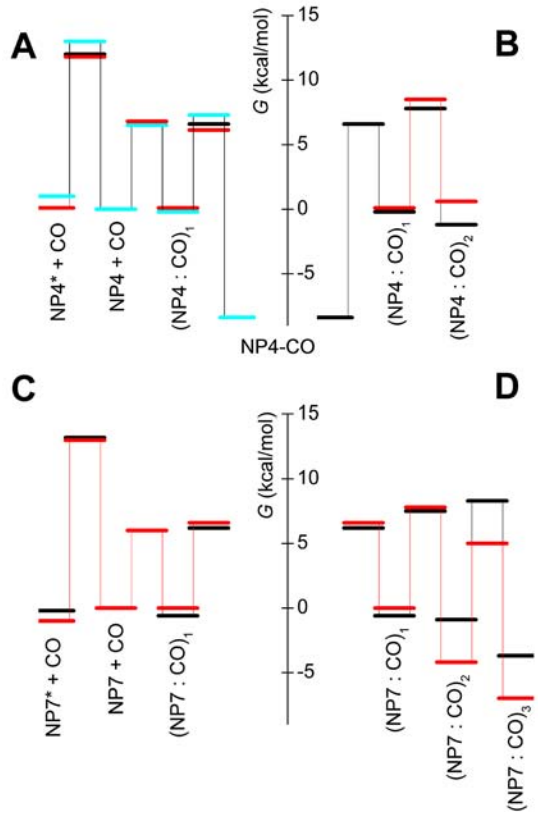

Figure 7. Free energy profiles for the CO migration and binding to NP4 solutions at 20 °C and pH 5.5 (red) and 7.5 (black, **c**; cyan, **o**). To allow better appreciation of the profiles, exit to solvent and structural rearrangement are reported in panel A, whereas migration through cavities is reported in panel B. Free energy of NP4 + CO was arbitrarily set to 0 and the energy of the bound state was accordingly calculated from the calorimetric data (see additional experimental details, Figure S7, and Table S5 in the Supporting Information).

Scheme 2. Minimal Reaction Scheme for the Observed CO Rebinding Kinetics to NP7 Solutions

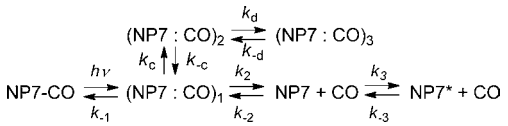

is difficult to estimate since much of the kinetics occurs within the dead time of the instrumentation. This fact leads to the apparent insensitivity of this step to the pH of the solution. Photodissociated ligands are stabilized in the temporary docking sites at acidic pH.

3.6. Determination of the CO Dissociation Reaction by Stopped-Flow Kinetic Measurements. The dissociation rate of CO from ferrohemes is typically very low ($\sim 10^{-2}$ s^{-1}).[37] In addition, because of the strong affinity, the dissociation rate cannot be determined by simple dilution experiments. Therefore, an excess of a stronger ligand, for example, NO (K_{eq} = 2.5 × 10^{12} M^{-1}),[15] can be used to shift the equilibrium to the side of the dissociated CO (K_{eq} = 4 × 10^6 M^{-1}, for NP4 at pH 7.5 and 20°C, see Supporting Information Table S5) according to Scheme 3.

The rate of this reaction follows the law

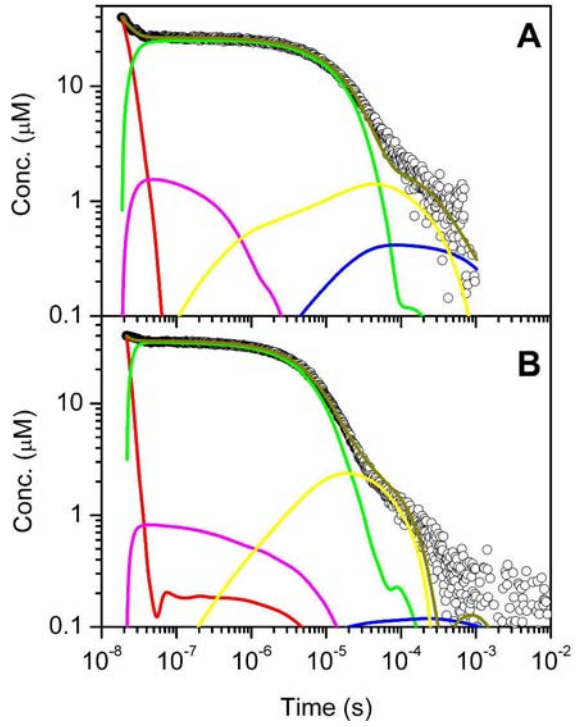

Figure 8. Representative fitting (dark yellow) with the model outlined in Scheme 2 for CO rebinding kinetics (○) to NP7 solutions at pH 5.5 (A) and 7.5 (B) at 25 °C and 1 atm CO. Reaction intermediates: red, $(NP7 : CO)_1$; magenta, $(NP7 : CO)_2$; yellow, $(NP7 : CO)_3$; blue, NP7*; green, NP7 (pH 5.5, 100 mM NaO*Ac*/HO*Ac*; pH 7.5, 100 mM MOPS/NaOH).

Scheme 3

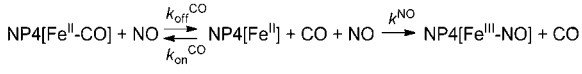

$$k_{obs} = \frac{k_{off}^{CO}}{1 + \frac{k_{on}^{CO}[CO]}{k_{on}^{NO}[NO]}} \quad (1)$$

Because [NO] ≫ [CO], it can be, in good approximation, assumed that $k_{obs} = k_{off}^{CO}$.

Samples of NP4−CO (~5 μM) were prepared under strictly anaerobic conditions. Excess of CO was removed from the solution by dialysis overnight where the integrity of the sample was checked before measurement by absorption spectroscopy. A second solution of the same buffer with an excess of DEA/NO (1 mM) was prepared and both solutions were kept inside the stopped-flow instrument's gastight syringes for an extensive time not only to reach a thermostatic equilibrium, but also to wait for a complete decomposition of DEA/NO into NO gas.[38] Measurements were then carried out at 20 °C and at 10 °C while the absorbance change at 421 nm was monitored. An example of the resulting kinetic traces is depicted in Figure 9.

In contrast to NP4[Fe^{II}], NP7[Fe^{II}] forms two species with His60-on and His60-off which are reflected in the appearance of two different Soret band absorptions, that is, ~422 and ~388 nm.[28] Consequently, NO is not a suitable competing ligand for the determination of CO off-rates of NP7. On the other hand, ferroheme NPs are remarkably quickly oxidized by O_2,[39] so that a thermostatted O_2 saturated solution ($[O_2]_{water}$ ≈ 1.4 mM at

dx.doi.org/10.1021/ja2121662 | J. Am. Chem. Soc. 2012, 134, 9986−9998

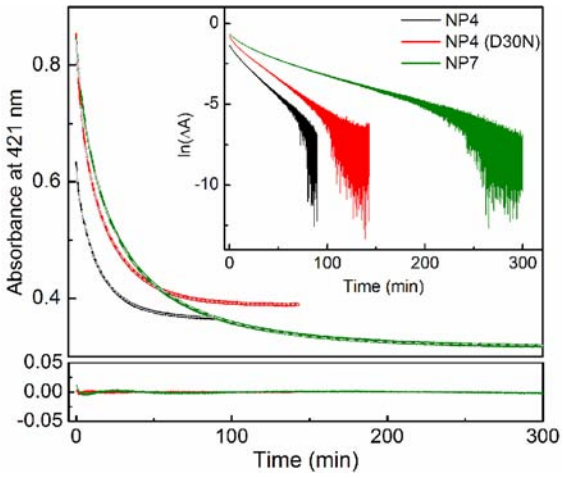

Figure 9. Reaction of ~5 μM NP4−CO and NP4(D30N)−CO with NO (saturated) or 5 μM NP7−CO with O_2 (saturated) in 100 mM MOPS/NaOH (pH 7.5) at 20 °C monitored by the absorbance change at 421 nm. Inset: Semilogarithmic plot of the data, the residual for the fit is shown at the bottom.

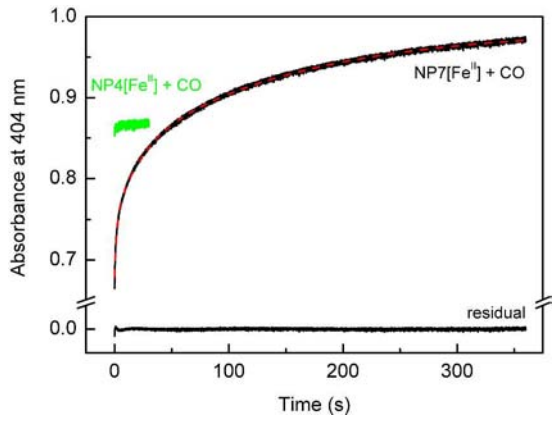

Figure 10. Kinetics of the association reaction of NP4[Fe^{II}] and NP7[Fe^{II}] with CO. Comparison of typical kinetic traces of NP4[Fe^{II}] + CO (green) and NP7[Fe^{II}] + CO (black). The fitting of the trace of NP7[Fe^{II}] + CO with three exponentials is given in red. Measurements were performed with 5 μM protein in 100 mM MOPS/NaOH (pH 7.5) mixed with CO saturated buffer at 10 °C.

25 °C and 1 atm)[26] was used to determine the CO dissociation rate according to Scheme 4.

Scheme 4

$$\text{NP7[Fe}^{II}\text{-CO]} + O_2 \underset{k_{on}^{CO}}{\overset{k_{off}^{CO}}{\rightleftharpoons}} \text{NP7[Fe}^{II}\text{]} + CO + O_2 \xrightarrow{k^{O_2}} \text{NP7[Fe}^{III}\text{]} + CO + O_2^{\bullet-}$$

This reaction sequence makes use of the fact that CO does not bind to ferrihemes. The formation of $O_2^{\bullet-}$ from this reaction has not been explicitly proven, but can be assumed by analogy with other heme proteins.[10c,40] The reaction is probably more complex than depicted in Scheme 4 because $O_2^{\bullet-}$ has itself a high oxidation potential; this is, however, not the topic of this investigation. Similar to eq 1, because of $[O_2] \gg [CO]$, $k_{obs} = k_{off}^{CO}$. Examples of the resulting kinetic traces are depicted in Figure 9.

In both cases, the kinetic traces had to be fit with a double exponential function to obtain a sufficient fit. This is evident also from the plot of $\ln(A_i - A_\infty)$ versus time which is also depicted in Figure 9 (inset). The resulting dissociation rates for the slow and the fast phase, k_{off}^{slow} and k_{off}^{fast}, are summarized in Supporting Information Table S4. A similar biphasic behavior was previously obtained for the dissociation of NO and histamine from NP1−4 and some site-directed mutants, including NP4(D30N) (compare Supporting Information Table S4).[12a,41]

3.7. Association Reaction of NP7[Fe^{II}] with CO. It was mentioned above that the reduction of NP7 with $S_2O_4^{2-}$ leads to the His60-on and His60-off species.[28] However, in the rapid LFP experiments, no indication for the breaking of the His−Fe^{II} bond was found. In addition to these experiments, the reaction of NP7[Fe^{II}] at equilibrium (NP7[Fe^{II}]$_{eq}$) was monitored by rapid-mixing stopped-flow experiments using various concentrations of CO. The experiments were repeatedly performed while the absorption was monitored close to both Soret band absorptions, that is, at 385, 404, and 421 nm. A typical kinetic trace recorded at 404 nm is presented in Figure 10. The kinetics trace comprises a very fast initial phase followed by a surprisingly long lasting process. The reaction of NP4[Fe^{II}] + CO at the same conditions is also displayed; as expected, this reaction proceeds at a time scale that is too fast for detection by a mixing experiment, which means that in the LFP experiments all details of the reaction are obtained.

The kinetic trace of NP7[Fe^{II}] + CO is only sufficiently fit by a three exponential function. The resulting rates contain a fast first phase of which the resulting rates k_{obs}^1 are in the range of >20 s^{-1}, too fast to be observed by the applied instrumentation. k_{obs}^2 and k_{obs}^3 are plotted versus [CO] in Supporting Information Figure S6 from the experiments monitored at 388 and 421 nm. As a result, both rates do not show dependence on [CO], which suggests that they reflect internal rearrangements rather than bimolecular interaction.

4. DISCUSSION

The transportation of NO by NPs involves the binding and the release of the NO molecule. The detailed understanding of the underlying dynamic processes is important to comprehend NP functionality, with implications that are of relevance for other NO binding and/or releasing heme proteins, like soluble guanylate cyclase (sGC), nitric oxide synthase (NOS), nitric oxide reductase (NOR), or heme cd_1 nitrite reductases (heme cd_1NiR), but also Mb and Hb. In particular, the latter two examples were heavily investigated by LFP experiments. In these cases, typically the CO complexes were applied as models, which is easier to follow because of the much slower binding and release rates compared to the NO complexes.

In the present study, a detailed analysis of the CO binding and release kinetics was performed on NP4, NP4(D30N), and NP7 where the two pHs relevant for the in vivo functionality of the NPs were considered. However, a major challenge in the LFP experiments is the interpretation of the kinetic traces. Therefore, in the present LFP study, the kinetic measurements were combined with FT-IR and RR spectroscopy, X-ray crystallography, stopped-flow kinetics, and isothermal microcalorimetry. Furthermore, whereas a preceding study focuses on the phase of geminate recombination in NP4,[42] the present study is dedicated mainly to the proper analysis of the slower time scales.

dx.doi.org/10.1021/ja2121662 | J. Am. Chem. Soc. 2012, 134, 9986−9998

4.1. CO Binding and Release Kinetics of NP4 at pH 5.5.

This is the easiest case among the NPs investigated in this study and will, therefore, be discussed first. CO rebinding after nanosecond photodissociation of NP4−CO is followed by geminate recombination with remarkably large amplitudes and apparent time constants of a few nanoseconds, close to the time resolution of the experimental setup. As previously reported,[42] a substantial part of the kinetics is lost within the instrumental dead-time, determined by the duration of the laser pulse of ∼7 ns.[43]

At pH 5.5, a kinetic model similar to the one typically applied for the globins[24] fits the data with sufficient accuracy. A single process is observed with $k_{-1} = 13 \times 10^7\ s^{-1}$. This rate is higher than those typically observed for other heme proteins, including human neuroglobin (Ngb) ($k_{-1} = 1.5 \times 10^7\ s^{-1}$),[23a] nonsymbiotic Hb from *Arabidopsis thaliana* (type 1, $k_{-1} = 0.51 \times 10^7\ s^{-1}$; type 2, $k_{-1} = 2.2 \times 10^7\ s^{-1}$),[23b] R state human HbA ($k_{-1} = 0.57 \times 10^7\ s^{-1}$),[23c] and Mb ($k_{-1} = 0.13 \times 10^7\ s^{-1}$).[23d] Since subnanosecond rebinding is not accessible to our experimental setup, the rates k_{-1} and k_2 are most underestimated and should be considered as lower limits. Combined analysis of nanosecond and picosecond experiments will allow a more precise determination of these rates. The bimolecular binding rate constant ($k_{ON} = k_{-2}k_{-1}/(k_{-1} + k_2)$) can be estimated from the microscopic rate constants as $k_{ON}(NP4) = 3.7 \times 10^7\ M^{-1}\ s^{-1}$.

The existence of an additional internal CO binding site (NP4 : CO)$_2$ had to be assumed in order to obtain a sufficient fitting of the experimental data (Scheme 1). The NP4 structure hosts two Xe cavities, designated Xe1 and Xe2,[33] which are apparently not populated by CO at cryogenic temperatures, as was demonstrated by FT-IR temperature derivative spectroscopy.[33] Subnanosecond geminate recombination of CO for NP4 solutions at room temperature is also not apparently modulated by Xe cavities.[42] However, on longer time scales, we found that temporary docking sites, probably Xe1/2, are populated near room temperature. The extent to which Xe1/2 in NP4 are populated is dependent on the pH of the solution, the population being larger at pH 7.5.

Signatures of ligand rebinding from temporary docking sites on the nano- to microsecond time scale are commonly found in the geminate phase of many Hbs. While in some cases rebinding from one or two docking sites is detectable,[23d] in other proteins very structured rebinding is observed as in human Ngb[23a] and in type 1 non symbiotic Hb from *A. thaliana*.[23e] Migration to the temporary docking site occurs with free energy barriers mostly determined by the entropic term.

It was previously noticed that the dissociation reaction of the NO release is heterogeneous in most of the NPs,[41] where *wt* NP7 is an exception.[9] An explanation for this heterogeneity remains, however, a matter of speculation.[13] Importantly, whereas for most heme proteins CO dissociation is monophasic, the protoglobin from *Methanosarcina acetivorans* represents another example where CO dissociation heterogeneity occurs.[44] In this respect, it has to be mentioned that previous attempts to handle the unliganded ferroheme NPs, for example, in stopped-flow kinetics, were not successful.[12b] We have recently presented that the rate of oxidation with O_2 is very fast (NP4: $k_{obs} = 2.8\ s^{-1}$ at 5 °C).[10c] However, by the insertion of the stopped-flow apparatus into an anaerobic chamber plus the installation of an anaerobic water thermostatting system, we successfully set up the stopped-flow experiment. The CO dissociation rates are of the typical order observed with heme proteins[37] and are much smaller compared to the NO dissociation rates. Interestingly, the heterogeneity observed with the NO complexes is also obtained with the CO complexes (Supporting Information Table S4). However, whereas the ratio of the amplitudes of the fast and the slow phases in case of NO dissociation from NP4 is typically ∼1, in case of the CO dissociation, it is ∼0.6. An explanation for this difference may be the different polarity of NO compared to the more polar CO molecule, which is expected to result in different interaction with the protein matrix.

4.2. Additional Location(s) for Ligand Docking in NP7.

In the case of NP7, the recovered rate k_{-1} is $6.9 \times 10^7\ s^{-1}$ at pH 7.5, but lowering the pH to 5.5 surprisingly leads to a slight decrease in this rate ($6.0 \times 10^7\ s^{-1}$). The latter finding is most likely an artifact, due to the fact that most of the kinetics falls below the time resolution of the experimental setup. CO migration through inner cavities is a more complex event in NP7, involving at least three reaction intermediates which can be interpreted as rebinding from temporary docking sites. The large barrier encountered by CO once docked into the very long-lived reaction intermediates means that the protein is in principle capable of effectively storing the gas for long times. This is even more evident in the pH 5.5 energetic profile (Figure 7), for which the free energies of the states (NP7 : CO)$_2$ and (NP7 : CO)$_3$ are much lower than the corresponding states at pH 7.5. Thus, stabilization is enhanced in the acidic conformation of the protein and reduced in the neutral pH conformation, a mechanism which may lead to facilitated release of the gas at increased pH.

Unfortunately, for NP7, an experimental structure is yet missing, although the homology model suggests an overall structure close to that of the other NPs.[9] Nevertheless, the CO association kinetics behave generally fairly similar to those of *wt* NP4. In agreement with the previous correlation between different CO conformers and rebinding processes, the kinetic trace of NP7 is sufficiently fit with a single set of parameters. Lowering the pH leads to an appreciable (3-fold) increase in the bimolecular binding rate constant for NP7, with values of $k_{ON} = 5 \times 10^7\ M^{-1}\ s^{-1}$ at pH 7.5 and $k_{ON} = 1.6 \times 10^8\ M^{-1}\ s^{-1}$ at pH 5.5, a fact that only partly accounts for the concomitant increase in affinity upon lowering the pH. In this case, NP7 NO dissociation heterogeneity is not observed.[9] However, in case of the CO dissociation reaction, two phases are obtained for both pHs with approximately equal amplitudes. Surprisingly, the reaction rates do principally not change for the two pHs applied.

We have recently shown that, in contrast to the other NP isoproteins, the reduction of NP7 leads to the partial breakage of the Fe−His60 bond at pH 7.5 as a result of the dense packing of side chains at the proximal heme site, which leads to the formation of a 5c water complex.[45,28] The equilibrium between the two states must perform through an intermediate, which can be the 4c unliganded form or the 6c water/His60 complex (see Scheme 5). However, the spectral features observed in RR spectroscopy of low-pH samples of NP7$[Fe^{II}]_{eq}$ support the presence of the 4c species,[28] so that we favor to consider this form as the transient species. As a consequence of the concomitant existence of 5c Fe−His and water−Fe, the total CO association reaction becomes very slow (minutes) where the trace was only sufficiently fit with three exponentials. The apparent value for k_{obs}^1 is too fast for the determination of

dx.doi.org/10.1021/ja2121662 | J. Am. Chem. Soc. 2012, 134, 9986−9998

Scheme 5. Coordination States in *wt* NP7[Fe^{II}] upon Binding and Release of CO

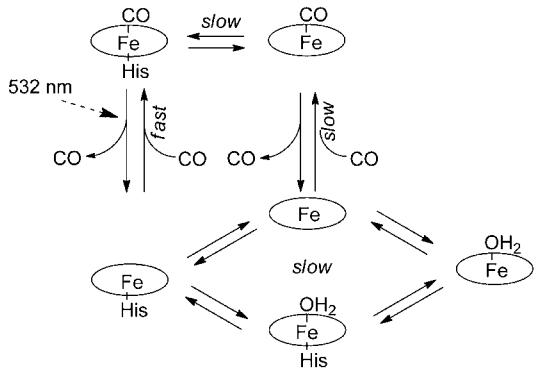

a meaningful value and reflects the association of CO to the Fe−His60 species like for NP4. Therefore, the slow phases k_{obs}^2 and k_{obs}^3 must reflect the association with the His60 unliganded form(s), which is assumed to be the 4c species.[46] In a second step, His60 will rebind to the Fe^{II} because in equilibrium only the 6c OC−Fe−His60 species is observed (see Supporting Information Figure S1). However, both the His association and dissociation are extremely slow processes and are, therefore, not observed in the LFP experiments. Furthermore, also the CO association to the 4c heme is a very slow reaction.[47]

4.3. Heterogeneity in the CO Recombination Kinetics of NP4 at pH 7.5. Where in the cases of NP4 at pH 5.5 and NP7 at pH 5.5 and 7.5 the LFP traces were sufficiently reproduced by a simple one-component model, this was not possible in the case of NP4 at pH 7.5. Therefore, to model the CO rebinding kinetics to NP4, it is important to take into account the expected heterogeneity, induced by the coexistence of open (**o**) and closed (**c**) conformations at neutral pH, as clearly indicated in the high resolution crystal structure of NP4.[12b] In previous FT-IR measurements of NP4[{FeNO}^{6}], two ν_{N-O} were obtained at 1908 and 1922 cm^{-1} which were associated with the presence of the two structural conformations.[33] Similarly, in the case of Mb−CO, two ν_{C-O} were used as reporters for the presence of an open and a closed conformation.[48] The presence of a single ν_{C-O} for NP4 at low pH, where only the closed conformation is observed, supports the interpretation of the two $\nu_{C-O}^{c,o}$ reflecting the closed and the open conformation.[49] The presence of more than one conformer was already noticed in a previous report where the absorbance of ν_{C-O} was fit with four Gaussian functions though it is not clear what the four bands should reflect.[33,42] However, the energies of the two major species in this case agree well with the two species obtained in the present study (see Figure 2 and Supporting Information Table S1). Furthermore, the ratios of the intensities of ν_{C-O}^c and ν_{C-O}^o are comparable and are also similar to those obtained for ν_{N-O} (4:1).[33]

In the X-ray structure of NP4−CO, only a single Fe−C−O conformer was obtained.[12b] Thus, the question arises what the two conformers obtained in solution represent. A most obvious effect is through the steric distortion of ∠(Fe−C−O), which is in the ideal case 180°.[30c] The simultaneous determination of ν_{Fe-C} and ν_{C-O} of NP4−CO at pH 7.5 with ^{12}CO and ^{13}CO allows the estimation of ∠(Fe−C−O) as is described by Spiro and Li[30c] yielding angles of 178° ± 5° for both cases, which is in good agreement with the 177° ± 1° reported for the NP4−CO X-ray structure at pH 5.6. It deviates, though, from the 173° ± 2° reported for the pH 7.4 X-ray structure; however, it is commented in this structural report that the occupancy of the O_{CO} was only 75% for unknown reasons, which may complicate the accurate model building and the accurate determination of the angle.[12b]

Multiple ν_{Fe-C}/ν_{C-O} pairs were already reported in the case of other heme proteins, in particular horse reddish peroxidase (HRP),[50] cytochrome *c* peroxidase (CCP) from baker's yeast,[51]

Scheme 6. Schematic Representation of the Molecular Arrangements Related to the CO Association/Dissociation of NP4 at pH 7.5[a]

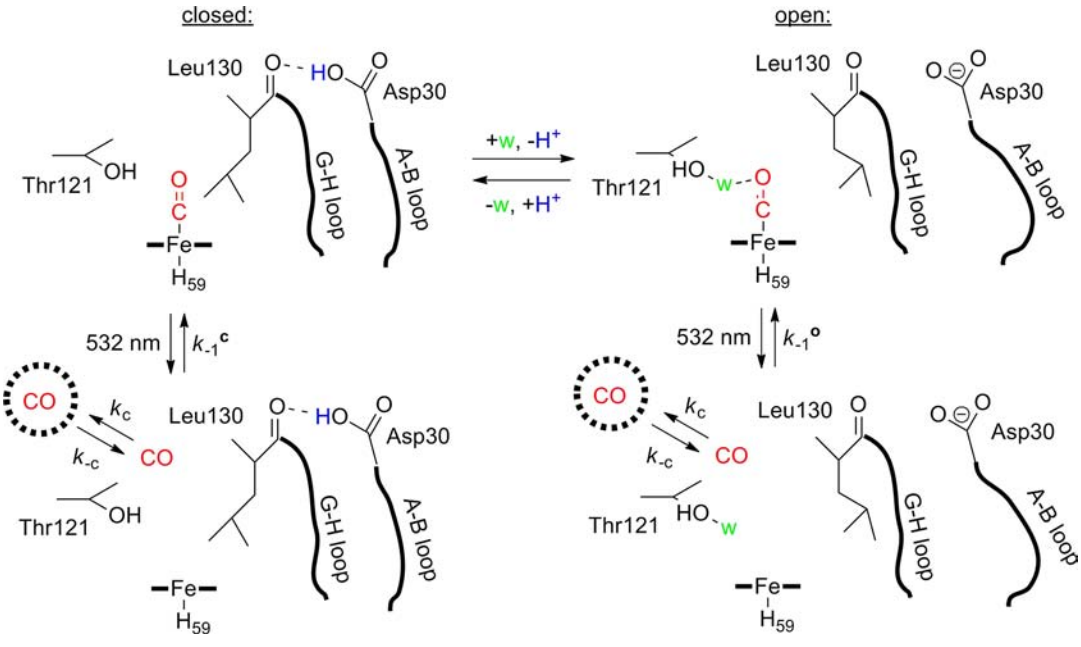

[a]w = crystallographically ordered water.

dx.doi.org/10.1021/ja2121662 | J. Am. Chem. Soc. 2012, 134, 9986−9998

and catalase peroxidase from *Mycobacterium tuberculosis* (KatG)[52] (see Figure 3 and Supporting Information Table S1). CCP(I) and CCP(II) as well as HRP(I) and HRP(III) exhibit a strong shifting to the P450 line as a result of the concomitant presence of imidazole and imidazolate character of the proximal His, as is demonstrated with PPDMe(ImH) and PPDMe(Im^-).[50] In contrast, NP4 shifts more parallel on the Mb line comparable to KatG(I) and KatG(II). This behavior is attributed to a difference in the CO environment, in particular $O_{CO}\cdots H^+$−base interaction. Though the X-ray structures of NP4−CO at pH 5.6 and 7.4 are very similar, two significant differences in the distal site exist. First of all, pH increase causes Leu130 to swing out from the front of the heme pocket as a consequence of Asp30 deprotonation, which breaks the Asp30···O=C_{Leu130} H-bond; thus, the distance $O_{CO} \leftrightarrow C^5_{Leu130}$ increases from 3.5 to 6.1 Å. Simultaneously, pH increase allows Thr121 in the back of the heme pocket to coordinate a water, that is then 3.4 Å distant to O_{CO}. It should be noted that the G-H loop was modeled in two conformations based on the high-resolution electron density of 1.0 Å where the open conformation (Leu130 moved out) had an occupancy of 0.55. It is well established that ν_{Fe-C}/ν_{C-O} is sensitive to environmental changes with the general trend that increasing polarity leads to decreased ν_{C-O}.[34a,53] The data suggest that the Thr121 bound water (w) may be responsible for the change in distal pocket polarity according to Scheme 6.

The model proposed herein to describe CO rebinding to NP4 takes into account the static heterogeneity by entering different reaction rates for the innermost rebinding step k_{-1} and structural relaxation k_3 and k_{-3}. The static heterogeneity is absent for NP4 at pH 5.5 and for NP7 at both pHs (Figures 1 and 2). CO rebinding to NP4 was recently investigated using pump and probe transient absorption methods with subnanosecond resolution.[42] The very large geminate phase, accounting for about 75% of the overall rebinding kinetics, was found to occur with a heterogeneous, nonexponential kinetics, which was described by the superposition of two processes, associated with rebinding to open and close conformations. The doming of the heme was held responsible for the nonexponential nature of the relaxations. Switching between the acidic (**c**) and the neutral (**o**) conformation changes the weight of the two kinetic processes.

The heterogeneity in the recovered rates for geminate rebinding to NP4 is responsible for the observed heterogeneous bimolecular binding rate constants, $k_{ON}^{c} = 4.5 \times 10^7\ M^{-1}\ s^{-1}$ and $k_{ON}^{o} = 1.9 \times 10^7\ M^{-1}\ s^{-1}$ that are very similar to that observed at pH 5.5 $k_{ON} = 3.7 \times 10^7\ M^{-1}\ s^{-1}$. Thus, unlike the case of NP7, for which lowering the pH results in a 3-fold increase in k_{ON}, for NP4, no major change in binding rate constant is observed. To confirm that the effect in heterogeneity is dictated by the loop conformation, the measurements were also performed with NP4(D30N). The NO dissociation kinetics of NP4(D30N) are very similar to those of the *wt* protein (Supporting Information Table S4); more importantly, a mixture of open and closed form of NP4(D30N) is also obtained in the X-ray structure at pH 5.6. Two ν_{C-O} and ν_{Fe-C} of similar frequency and amplitude as for *wt* NP4 at pH 7.5 are consistently obtained, thus, indicating that a similar ground state compound exists with respect to the Fe−CO. The significant difference with this protein is the persistence of the static heterogeneity also at pH 5.5. Moreover, it shows that the geminate rebinding as well as the bimolecular kinetics are not affected by the different A-B loop behavior at low and high pH (Supporting Information Table S2).

5. CONCLUSIONS

In summary, in this study, strong evidence for the existence of gas ligand hosting cavities in nitrophorins is found. This is in contrast to the interpretation of data of some previous examinations of NP4, which were performed only on the ultrafast kinetics (geminate phase),[42] on frozen solutions at very low temperature and high pH,[33] and in silico.[13] We have extended our research on low and high pH and included the mutant NP4(D30N) as well as *wt* NP7. The data agree excellently with the existence of two Xe hosting cavities in the X-ray structure of NP4.[33] The first examination of NP7 in that respect reveals the presence of secondary docking sites that are remarkably more effective than NP4 in storing the photodissociated CO, where the Fe^{II}−CO complex can be used as a model for the native {FeNO}^{6} complex. The presence of more internal gas hosting capacity in NP7 compared to NP4 is an interesting fact with respect to the unique ability of NP7 to bind to negatively charged cell membranes.[5b,54] One hypothesis for the functional meaning is to support the delivery of NO close to a target cell for which the presence of NO hosting cavities might be important.

Another important finding is the surprisingly small change in the free energy barriers throughout the rebinding and release pathway upon increase of the pH in case of NP4. This is in marked contrast to the MD simulations in which a large free energy barrier for the low pH was predicted that was markedly decreased at high pH.[13] While it is certainly true that in the present study CO was used, whereas the in silico investigations considered NO, it is hard to imagine that the difference between the two diatomic gas molecules would be so large that interactions with the protein matrix would be energetically entirely different. On the other hand, in case of NP7, a large change in the free energy barriers was obtained for the inner docking sites dependent on the pH. It is interesting to note that in case of NP4 the pH dependent change in K_{eq} is relatively small ($20 \times 10^6\ M^{-1} \rightarrow 5 \times 10^6\ M^{-1}$).[15] Thus, the question might be posted to which extent the release mechanism in vivo is simply diffusion controlled, that is, if the mechanism of NO delivery is not more complex.[10c] It was suggested that blood histamine could be an in vivo-heme ligand competing with NO.[11] However, where K_{eq}(histamine) of NP1−4 (1×10^8 to $1.3 \times 10^7\ M^{-1}$) compared to the plasma histamine concentrations (1−10 nM)[55] supports such a scenario, K_{eq}(histamine) of NP7 is too small ($1 \times 10^5\ M^{-1}$). In this respect, one should consider the interaction of NP2 with factor Xase complex[56] and the interaction of NP7 with cell membranes,[5b,55] pointing toward a more complex in vivo scenario where the presence of internal gas docking sites might facilitate the modulation of NO release through interaction with blood components.

Overall, this first study on the slow phase of the dynamics of diatomic gas molecule interaction with NPs is a contribution to the understanding of the function of NPs as NO transporting molecules. Moreover, the handling and specific targeting of the delicate signaling molecule NO in biological systems is little understood. The study of the native NO transporter NP represents, therefore, an important target to understand the principles of molecular architecture profitable for the delivery of NO in biology and even pharmacology.

■ ASSOCIATED CONTENT

Supporting Information

Additional experimental details; Figure S1, absorbance spectra of NP7; Figure S2, RR spectra of ^{12}CO and ^{13}CO bound NP4; Figure S3, CO rebinding kinetics at $p(CO)$ = 1 and 0.1 atm; Figure S4, time-resolved spectra of NP4-CO; Figure S5, CO rebinding kinetics obtained for NP4(D30N); Figure S6, concentration dependence of NP7 + CO association reaction; Figure S7, isothermal microcalorimetry of NP4 + CO; Table S1, collection of ν_{C-O} and ν_{Fe-C}; Tables S2−S3, rate constants and activation enthalpies and entropies; Table S4, CO dissociation rates; Table S5, thermodynamic parameters of the NP4 + CO association. This material is available free of charge via the Internet at http://pubs.acs.org.

■ AUTHOR INFORMATION

Corresponding Author

cristiano.viappiani@fis.unipr.it; markus.knipp@mpi-mail.mpg.de

Notes

The authors declare no competing financial interest.

■ ACKNOWLEDGMENTS

The authors thank Johanna J. Taing, Leslie Currel, Jan Hanis, Robyn L. Kosinsky, Marion Stapper, Alessandro Tinozzi, and Pietro Delcanale for their technical assistance. Prof. F. Ann Walker (Department of Chemistry and Biochemistry, University of Arizona, Tucson, AZ) is acknowledged for the gift of the expression vectors for *wt* NP4 and *wt* NP7. This work was financially supported by the Vigoni Program, Project E65E06000080001, (to C.V.), the Deutscher Akademischer Austausch Dienst (DAAD), Project 50728589, (to M.K.), and the Max Planck Society (MPG) (to M.K.).

■ REFERENCES

(1) Abbreviations used: 4c, 4-coordinate; 5c, 5-coordinate; 6c, 6-coordinate; CCP, cytochrome c peroxidase from baker's yeast; DEA/NO, diethylammonium 2-(*N*,*N*-diethylamino)diazenolate-2- oxide; Hb, hemoglobin; HRP, horse radish peroxidase; HS, high-spin; ImH, imidazole; KatG, catalase peroxidase from *Mycobacterium tuberculosis*; LFP, laser-flash photolysis; LS, low-spin; Mb, myoglobin; MALDI, matrix assisted laser desorption/ionization; MEM, Maximum Entropy Method; MOPS, 3-mopholino-1-propanesulfonic acid; Ngb, neuroglobin; NiR, nitrite reductase; NMWL, nominal molecular weight limit; NOS, nitric oxide synthase; NOR, nitric oxide reductase; NP, nitrophorin; P450, cytochrome P-450; PPDMe, protoporphyrin IX dimethyl ester; PDB, RSCB protein database at http://www.rscb.org/; RMSD, root mean square deviations; RR, resonance Raman; sGC, soluble guanylate cyclase; SVD, singular value decomposition; TOF, time-of-flight; *wt*, wildtype.

(2) Lehane, M. J. *The Biology of Blood-Sucking in Insects*; 2 ed.; Cambridge University Press: Cambridge, United Kingdom, 2005.

(3) (a) Ribeiro, J. M. C.; Hazzard, J. M.; Nussenzveig, R. H.; Champagne, D. E.; Walker, F. A. *Science* **1993**, *260*, 539−541. (b) Andersen, J. F.; Gudderra, N. P.; Francischetti, I. M. B.; Ribeiro, J. M. C. *Arch. Insect Biochem. Physiol.* **2005**, *58*, 97−105.

(4) (a) Andersen, J. F.; Champagne, D. E.; Weichsel, A.; Ribeiro, J. M. C.; Balfour, C. A.; Dress, V.; Montfort, W. R. *Biochemistry* **1997**, *36*, 4423−4428. (b) Andersen, J. F.; Montfort, W. R. *J. Biol. Chem.* **2000**, *275*, 30496−30503.

(5) (a) Andersen, J. F.; Gudderra, N. P.; Francischetti, I. M. B.; Valenzuela, J. G.; Ribeiro, J. M. C. *Biochemistry* **2004**, *43*, 6987−6994. (b) Knipp, M.; Zhang, H.; Berry, R. E.; Walker, F. A. *Protein Expression Purif.* **2007**, *54*, 183−191.

(6) Knipp, M.; Soares, R. P. P.; Pereira, M. H. *Anal. Biochem.* **2012**, *424*, 79−81.

(7) Walker, F. A. *J. Inorg. Biochem.* **2005**, *99*, 216−236.

(8) Soares, A. C.; Carvalho-Tavares, J.; Gontijo, N. d. F.; dos Santos, V. C.; Teixeira, M. M.; Pereira, M. H. *J. Insect Physiol.* **2006**, *52*, 468−472.

(9) Knipp, M.; Yang, F.; Berry, R. E.; Zhang, H.; Shokhirev, M. N.; Walker, F. A. *Biochemistry* **2007**, *46*, 13254−13268.

(10) (a) He, C.; Knipp, M. *J. Am. Chem. Soc.* **2009**, *131*, 12042−12043. (b) He, C.; Ogata, H.; Knipp, M. *Biochemistry* **2010**, *49*, 5841−5851. (c) Knipp, M.; He, C. *IUBMB Life* **2011**, *63*, 304−312.

(11) Weichsel, A.; Andersen, J. F.; Champagne, D. E.; Walker, F. A.; Montfort, W. R. *Nat. Struct. Biol.* **1998**, *5*, 304−309.

(12) (a) Maes, E. M.; Weichsel, A.; Andersen, J. F.; Shepley, D.; Montfort, W. R. *Biochemistry* **2004**, *43*, 6679−6690. (b) Maes, E. M.; Roberts, S. A.; Weichsel, A.; Montfort, W. R. *Biochemistry* **2005**, *44*, 12690−12699. (c) Kondrashov, D. A.; Roberts, S. A.; Weichsel, A.; Montfort, W. R. *Biochemistry* **2004**, *43*, 13637−13647. (d) Weichsel, A.; Andersen, J. F.; Roberts, S. A.; Montfort, W. R. *Nat. Struct. Biol.* **2000**, *7*, 551−554. (e) Roberts, S. A.; Weichsel, A.; Qiu, Y.; Shelnutt, J. A.; Walker, F. A.; Montfort, W. R. *Biochemistry* **2001**, *40*, 11327−11337. (f) Andersen, J. F.; Weichsel, A.; Balfour, C. A.; Champagne, D. E.; Montfort, W. R. *Structure* **1998**, *6*, 1315−1327.

(13) Swails, J. M.; Meng, Y.; Walker, F. A.; Martí, M. A.; Estrin, D. A.; Roitberg, A. E. *J. Phys. Chem. B* **2009**, *113*, 1192−1201.

(14) Hoshino, M.; Maeda, M.; Konishi, R.; Seki, H.; Ford, P. C. *J. Am. Chem. Soc.* **1996**, *118*, 5702−5707.

(15) Berry, R. E.; Shokhirev, M. N.; Ho, A. Y. W.; Yang, F.; Shokhireva, T. K.; Zhang, H.; Weichsel, A.; Montfort, W. R.; Walker, F. A. *J. Am. Chem. Soc.* **2009**, *131*, 2313−2327.

(16) Shokhireva, T. K.; Berry, R. E.; Uno, E.; Balfour, C. A.; Zhang, H.; Walker, F. A. *Proc. Natl. Acad. Sci. U.S.A.* **2003**, *100*, 3778−3783.

(17) Ding, X. D.; Weichsel, A.; Andersen, J. F.; Shokhireva, T. K.; Balfour, C.; Pierik, A. J.; Averill, B. A.; Montfort, W. R.; Walker, F. A. *J. Am. Chem. Soc.* **1999**, *121*, 128−138.

(18) Traylor, T. G.; Sharma, V. S. *Biochemistry* **1992**, *31*, 2847−2849.

(19) Ignarro, L. J. *Annu. Rev. Pharmacol. Toxicol.* **1990**, *30*, 535−560.

(20) (a) Subczynski, W. K.; Lomnicka, M.; Hyde, J. S. *Free Radical Res.* **1996**, *24*, 343−349. (b) Huang, K. T.; Huang, Z.; Kim-Shapiro, D. B. *Nitric Oxide* **2007**, *16*, 209−216. (c) Chakraborty, S.; Balakotaiah, V.; Bidani, A. *J. Appl. Physiol.* **2004**, *97*, 2284−2302.

(21) (a) Knipp, M. *ChemBioChem* **2006**, *7*, 879−889. (b) Pervin, S.; Chaudhuri, G.; Singh, R. *Curr. Pharm. Des.* **2010**, *16*, 451−462.

(22) (a) Coulter, J. A.; McCarthy, H. O.; Xiang, J.; Roedl, W.; Wagner, E.; Robson, T.; Hirst, D. G. *Nitric Oxide* **2008**, *19*, 192−198. (b) Chen, C.; Shi, Y.; Li, S.; Qi, Q.; Gu, L.; Song, J.; Wang, P. G. *Arch. Pharm. Chem. Life Sci.* **2006**, *339*, 366−371.

(23) (a) Abbruzzetti, S.; Faggiano, S.; Bruno, S.; Spyrakis, F.; Mozzarelli, A.; Dewilde, S.; Moens, L.; Viappiani, C. *Proc. Natl. Acad. Sci. U.S.A.* **2009**, *106*, 18984−18989. (b) Bruno, S.; Faggiano, S.; Spyrakis, F.; Mozzarelli, A.; Abbruzzetti, S.; Grandi, E.; Viappiani, C.; Feis, A.; Mackowiak, S.; Smulevich, G.; Cacciatori, E.; Dominici, P. *J. Am. Chem. Soc.* **2007**, *129*, 2880−2889. (c) Henry, E. R.; Bettati, S.; Hofrichter, J.; Eaton, W. A. *Biophys. Chem.* **2002**, *98*, 149−164. (d) Sottini, S.; Abbruzzetti, S.; Viappiani, C.; Ronda, L.; Mozzarelli, A. *J. Phys. Chem. B* **2005**, *109*, 19523−19528. (e) Abbruzzetti, S.; Grandi, E.; Bruno, S.; Faggiano, S.; Spyrakis, F.; Mozzarelli, A.; Dominici, P.; Viappiani, C. *J. Phys. Chem. B* **2007**, *111*, 12582−12590.

(24) Abbruzzetti, S.; Bruno, S.; Fagiano, S.; Grandi, E.; Mozzarelli, A.; Viappiani, C. *Photochem. Photobiol. Sci.* **2006**, *5*, 1109−1120.

(25) Sottini, S.; Viappiani, C.; Ronda, L.; Bettati, S.; Mozzarelli, A. *J. Phys. Chem. B* **2004**, *108*, 8475−8484.

(26) *CRC Handbook of Chemistry and Physics*; 67 ed.; Weast, R. C., Astle, M. J., Beyer, W. H., Eds.; CRC Press, Inc.: Boca Raton, FL, 1986−1987.

(27) Knipp, M.; Taing, J. J.; He, C. *J. Inorg. Biochem.* **2011**, *105*, 1405−1412.

(28) He, C.; Neya, S.; Knipp, M. *Biochemistry* **2011**, *50*, 8559−8575.

(29) Decatur, S. M.; Franzen, S.; DePillis, G. D.; Dyer, R. B.; Woodruff, W. H.; Boxer, S. G. *Biochemistry* **1996**, *35*, 4939−4944.
(30) (a) Maes, E. M.; Walker, F. A.; Montfort, W. R.; Czernuszewicz, R. S. *J. Am. Chem. Soc.* **2001**, *123*, 1164−1172. (b) Kincaid, J. R. In *The Porphyrin Handbook*; 1st ed.; Kadish, K. M., Smith, K. M., Guilard, R., Eds.; Academic Press: San Diego, CA, 2000; Vol. *7*, pp 225−291; (c) Spiro, T. G.; Li, X.-Y. In *Resonance Raman Spectra of Heme and Metalloproteins*; 1st ed.; Spiro, T. G., Ed.; John Wiley & Sons: New York, 1988; pp 1−38; (d) Andersson, L. A.; Mylrajan, M.; Sullivan, E. P., Jr.; Strauss, S. H. *J. Biol. Chem.* **1989**, *264*, 19099−19102. (e) Kitagawa, T.; Kyogoku, Y.; Iizuka, T.; Saito, M. I. *J. Am. Chem. Soc.* **1976**, *98*, 5169−5173.
(31) Spiro, T. G.; Stong, J. D.; Stein, P. *J. Am. Chem. Soc.* **1979**, *101*, 2648−2655.
(32) (a) Palaniappan, V.; Bocian, D. F. *Biochemistry* **1994**, *33*, 14264−14274. (b) Tang, Q.; Kalsbeck, W. A.; Olson, J. S.; Bocian, D. F. *Biochemistry* **1998**, *37*, 7047−7056. (c) Sage, J. T.; Morikis, D.; Champion, P. M. *Biochemistry* **1991**, *30*, 1227−1237.
(33) Nienhaus, K.; Maes, E. M.; Weichsel, A.; Montfort, W. R.; Nienhaus, G. U. *J. Biol. Chem.* **2004**, *279*, 39401−39407.
(34) (a) Yu, N.-T.; Kerr, E. A. In *Biological Applications of Raman Spectroscopy. Resonance Raman Spectra of Heme and Metalloproteins*; 1st ed.; Spiro, T. G., Ed.; John Wiley & Sons: New York, NY, 1988; Vol. *3*, pp 39−95; (b) Spiro, T. G.; Wasbotten, I. H. *J. Inorg. Biochem.* **2005**, *99*, 34−44.
(35) Vogel, K. M.; Kozlowski, P. M.; Zgierski, M. Z.; Spiro, T. G. *Inorg. Chim. Acta* **2000**, *297*, 11−17.
(36) (a) Jung, C.; Hui Bon Hoa, G.; Schroeder, K. L.; Simon, M.; Doucet, J. P. *Biochemistry* **1992**, *31*, 12855−12862. (b) Uno, T.; Nishimura, Y.; Makino, R.; Iizuka, T.; Ishimura, Y.; Tsuboi, M. *J. Biol. Chem.* **1985**, *260*, 2023−2026.
(37) Abbruzzetti, S.; Sottini, S.; Viappiani, C.; Corrie, J. E. T. *J. Am. Chem. Soc.* **2005**, *127*, 9865−9874.
(38) Maragos, C. M.; Morley, D.; Wink, D. A.; Dunams, T. M.; Saavedra, J. E.; Hoffman, A.; Bove, A. A.; Isaac, L.; Hrabie, J. A.; Keefer, L. K. *J. Med. Chem.* **1991**, *34*, 3242−3247.
(39) Knipp, M.; He, C.; Ogata, H. *Nitric Oxide* **2011**, *24* (Suppl.), S33−S34.
(40) (a) Riess, J. G. *Chem. Rev.* **2001**, *101*, 2797−2919. (b) George, P.; Stratmann, C. J. *Biochem. J.* **1954**, *57*, 568−573. (c) Shikama, K. *Chem. Rev.* **1998**, *98*, 1357−1373.
(41) Andersen, J. F.; Ding, X. D.; Balfour, C.; Shokhireva, T. K.; Champagne, D. E.; Walker, F. A.; Montfort, W. R. *Biochemistry* **2000**, *39*, 10118−10131.
(42) Benabbas, A.; Ye, X.; Kubo, M.; Zhang, Z.; Maes, E. M.; Montfort, W. R.; Champion, P. M. *J. Am. Chem. Soc.* **2010**, *132*, 2811−2820.
(43) Incidentally, we wish to point out that this holds also for NP7.
(44) Nardini, M.; Pesce, A.; Thijs, L.; Saito, J. A.; Dewilde, S.; Alam, M.; Ascenzi, P.; Coletta, M.; Ciaccio, C.; Moens, L.; Bolognesi, M. *EMBO Rep.* **2008**, *9*, 157−163.
(45) This can be seen by the appearance of the high-energy Soret absorbance of NP7[Fe^{II}] in Supporting Information Figure S1.
(46) A similar behavior of ferroheme NP7 is even seen in the oxidation reaction with O_2 as compared to ferroheme NP4.[10c]
(47) (a) Larsen, R. W.; E., W. P.; Findsen, E. W. *Inorg. Chim. Acta* **2001**, *319*, 1−7. (b) Kharitonov, V. G.; Sharma, V. S.; Pilz, R. B.; Magdet, D.; Koesling, D. *Proc. Natl. Acad. Sci. U.S.A.* **1995**, *92*, 2568−2571.
(48) (a) Mueller, J. D.; McMahon, B. H.; Chien, E. Y.; Sligar, S. G.; Nienhaus, G. U. *Biophys. J.* **1999**, *77*, 1036−1051. (b) Sage, J. T.; Morikis, D.; Champion, P. M. *Biochemistry* **1991**, *30*, 1227−1237.
(49) The two conformations are further reflected in the two ν_{Fe-C} modes obtained in RR spectroscopy (Figure 1). However, FT-IR allows the relative quantification of the two species.
(50) Evangelista-Kirkup, R.; Smulevich, G.; Spiro, T. G. *Biochemistry* **1986**, *25*, 4420−4425.
(51) Smulevich, G.; Evangelista-Kirkup, R.; English, A.; Spiro, T. G. *Biochemistry* **1986**, *25*, 4426−4430.
(52) Lukat-Rodgers, G. S.; Wengenack, N. L.; Rusnak, F.; Rodgers, K. R. *Biochemistry* **2001**, *40*, 7149−7157.
(53) (a) Xu, C.; Ibrahim, M.; Spiro, T. G. *Biochemistry* **2008**, *47*, 2379−2387. (b) Silvernail, N. J.; Roth, A.; Schulz, C. E.; Noll, B. C.; Scheidt, W. R. *J. Am. Chem. Soc.* **2005**, *127*, 14422−14433.
(54) Andersen, J. F.; Gudderra, N. P.; Francischetti, I. M. B.; Valenzuela, J. G.; Ribeiro, J. M. C. *Biochemistry* **2004**, *43*, 6987−6994.
(55) Jochem, J.; Żwirska-Korczala, K. W. In *Histamine: Biology and Medical Aspects*; Falus, A., Grosman, N., Darvas, Z., Eds.; SpringMed Publishing Ltd.: Budapest, Hungary, 2004; pp 303−316.
(56) (a) Ribeiro, J. M. C.; Schneider, M.; Guimarães, J. A. *Biochem. J.* **1995**, *308*, 243−249. (b) Gudderra, N. P.; Ribeiro, J. M. C.; Andersen, J. F. *J. Biol. Chem.* **2005**, *280*, 25022−25028.